Hill, T. L., Green, P. L., Cammarano, A., & Neild, S. A. (2016). Fast Bayesian identification of a class of elastic weakly nonlinear systems using backbone curves. Journal of Sound and Vibration, 360, 156-170. 10.1016/j.jsv.2015.09.007

Journal of Sound and Vibration 360 (2016) 156–170

Contents lists available at ScienceDirect

Journal of Sound and Vibration

journal homepage: www.elsevier.com/locate/jsvi

Fast Bayesian identification of a class of elastic weakly nonlinear systems using backbone curves

T.L. Hill [a,*], P.L. Green [b], A. Cammarano [c], S.A. Neild [a]

[a] Department of Mechanical Engineering, Queen's Building, University of Bristol, Bristol BS8 1TR, UK
[b] Institute for Risk and Uncertainty, School of Engineering, University of Liverpool, Liverpool L69 3GQ, UK
[c] School of Engineering, University of Glasgow, Glasgow G12 8QQ, UK

ARTICLE INFO

Article history:
Received 19 December 2014
Received in revised form
13 June 2015
Accepted 6 September 2015
Handling Editor: W. Lacarbonara
Available online 28 September 2015

ABSTRACT

This paper introduces a method for the identification of the parameters of nonlinear structures using a probabilistic Bayesian framework, employing a Markov chain Monte Carlo algorithm. This approach uses analytical models to describe the unforced, undamped dynamic responses of structures in the frequency–amplitude domain, known as the *backbone curves*. The analytical models describing these backbone curves are then fitted to measured responses, found using the *resonant-decay method*. To investigate the proposed identification method, a nonlinear two-degree-of-freedom example structure is simulated numerically and analytical expressions describing the backbone curves are found. These expressions are then used, in conjunction with the backbone curve data found through simulated experiment, to estimate the system parameters. It is shown that the use of these computationally-cheap analytical expressions allows for an extremely efficient method for modelling the dynamic behaviour, providing an identification procedure that is both fast and accurate. Furthermore, for the example structure, it is shown that the estimated parameters may be used to accurately predict the existence of dynamic behaviours that are well-away from the backbone curve data provided; specifically the existence of an isola is predicted.

1. Introduction

As nonlinear behaviour in structural dynamics becomes increasingly important, so does the need to accurately describe its characteristics. Whilst a number of reliable and efficient approaches have been developed for the identification of the linear characteristics of nonlinear systems, for example [1,2], the identification of nonlinearities still poses a number of challenges. Existing approaches to the problem in multi-degree-of-freedom systems include the restoring force method [3], NARMAX methods [4] and the conditioned reverse path method [5]. An extensive review of these, and other approaches, is given in [6]. Methods that are of specific interest to this work include the nonlinear resonant decay method [7,8], and the use of Bayesian approaches [9–12].

Bayesian methods for parameter identification problems seek to determine the probability that a particular set of parameter values are "correct", given some experimental data. The resulting probability density function, referred to as the *posterior*, is difficult to find analytically for nonlinear systems. Alternatively a Markov chain Monte Carlo (MCMC) method

* Corresponding author.
E-mail address: tom.hill@bristol.ac.uk (T.L. Hill).

http://dx.doi.org/10.1016/j.jsv.2015.09.007
0022-460X/

may be used, alongside simulations of the system, to sample from the posterior. Due to the complexity of modelling nonlinear systems, these simulations often require numerical integration through time at great computational expense. This issue can be mediated, to an extent, through the use of surrogate models and algorithms which are suitable for parallelisation [13,14], or through using carefully selected subsets of the experimental data [12,15]. However, computational expense still proves limiting for the application of these Bayesian methods to large nonlinear systems with many unknown parameters.

In this paper, a method is introduced that allows Bayesian system identification to be conducted in a computationally efficient manner without the need for model surrogates, or the need to use fewer experimental data. The method proposed here relies on inferring parameter estimates from experimentally measured *backbone curves* (i.e. the unforced, undamped response of nonlinear systems) and analytical expressions describing the curves. This approach results in significantly lower computational expense than those using time-domain numerical models.

Two nonlinear oscillators, each with two degrees-of-freedom, are considered in this work. These are introduced in Section 2, along with a procedure for the acquisition of data describing the backbone curves. This procedure is similar to the resonant decay method, as detailed in [8]. A number of techniques may be used for developing analytical models for the backbone curves; for example, harmonic balancing, multiple scales or the first-order normal form technique [16–18]. Here, however, we use the second-order normal form technique [19] as it is not only able to analytically describe modal interactions in backbone curves [20,21], but it is also suited for automation due to its matrix-based formulation – an essential property for the identification of larger systems. A brief outline of the application of the second-order normal form technique to the example system is given in Section 3, and further details are provided in Appendix A.

Section 4 is dedicated to the discussion of the Bayesian parameter estimation approach taken here, with specific details regarding the formulation adopted to accommodate the analytical model. This discussion also examines the use of the residuals of the expressions describing the backbone curves, thus eliminating the need for explicit solutions which can be computationally demanding to calculate. The results of the parameter identification for the example systems are presented in Section 5 where it is shown that the predictions of the responses of the system, made using the estimated parameters, are accurate in response regions well-away from those described by the data. Specifically, backbone curves that are not described by the measured data can be obtained, using the estimated parameters – demonstrated here by the prediction of an isola. Finally, conclusions are drawn in Section 6 and discussion is given to the potential future applications of the approach outlined in this work.

2. Measuring backbone curves

2.1. The example systems

Fig. 1 shows a two-degree-of-freedom oscillator with a symmetric, linear structure and three nonlinear springs. The underlying linear structure is composed of two identical springs and viscous dampers that ground the masses, as well as a spring and a viscous damper connecting the masses. The grounding springs and connecting spring have stiffness constants k_1 and k_2 respectively, and the grounding dampers and connecting damper have damping constants c_1 and c_2 respectively. Additionally, two nonlinear cubic springs, with constants α_1 and α_3, ground the masses and a nonlinear cubic spring, with constant α_2, connects the masses. The two masses have displacements x_1 and x_2, and both are of mass m. Sinusoidal forcing at frequency Ω_f is applied to the masses at amplitudes P_1 and P_2 as shown.

The equation of motion for this system may be written as

$$\mathbf{M}\ddot{\mathbf{x}}+\mathbf{C}\dot{\mathbf{x}}+\mathbf{K}\mathbf{x}+\mathbf{\Gamma}_x(\mathbf{x})=\mathbf{P}_x\ \cos(\Omega_f t), \tag{1}$$

where $\mathbf{M}$, $\mathbf{C}$ and $\mathbf{K}$ are $\{2\times 2\}$ mass, damping and stiffness matrices, respectively. The $\{2\times 1\}$ vectors $\mathbf{x}$, $\mathbf{\Gamma}_x$ and $\mathbf{P}_x$ describe the physical displacements, nonlinear terms and the forcing amplitudes respectively, and are written as

$$\mathbf{x}=\begin{pmatrix}x_1\\x_2\end{pmatrix},\quad \mathbf{\Gamma}_x=\begin{pmatrix}\alpha_1x_1^3+\alpha_2(x_1-x_2)^3\\\alpha_3x_2^3+\alpha_2(x_2-x_1)^3\end{pmatrix},\quad \mathbf{P}_x=\begin{pmatrix}P_1\\P_2\end{pmatrix}. \tag{2}$$

In this paper, two different parameter sets for the oscillator shown in Fig. 1 are considered. These parameter sets, labelled 1*NL* and 3*NL*, are given in Table 1. Parameter set 1*NL* describes a system that has previously been investigated in [22], and

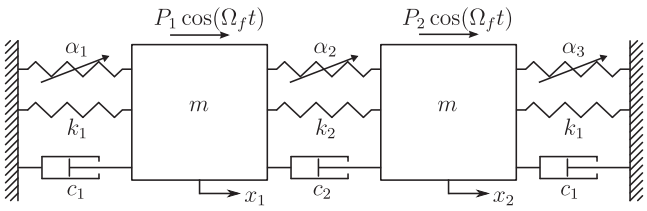

Fig. 1. A schematic diagram of an in-line, two-degree-of-freedom oscillator with a symmetric linear structure and three nonlinear cubic springs.

Table 1
The parameter values used in the two example systems, 1*NL* and 3*NL*.

Parameter	m	c_1	c_2	k_1	k_2	α_1	α_2	α_3
1***NL***	1	0.002	0.001	1	1	0.5	0	0
3***NL***	1	0.002	0.001	1	0.105	0.5	0.05	0.4

has only one nonlinear spring, i.e. $\alpha_2 = \alpha_3 = 0$. Parameter set 3*NL* describes a system with three nonlinear springs, i.e. all nonlinear parameters are non-zero. Aside from the nonlinear coefficient, the only parameter that differs between the two systems is the coefficient of the linear spring connecting the masses, k_2, resulting in different linear natural frequencies between 1*NL* and 3*NL*. As the parameters describing the external forcing – P_1, P_2 and Ω_f – are not characteristics of the physical system, they are not listed in Table 1. Furthermore, for the technique presented here, it is not necessary for the external forces to be measured. Instead, the forcing parameters are defined whenever a forced response is considered.

2.2. An experimental method for measuring backbone curves

The data used for the identification process in this paper have been collected through simulated experiment. This employs a numerical integration routine, specifically MATLAB's integration algorithm implementing Runge–Kutta (4,5) [23], to simulate the procedure detailed below. Additionally, Gaussian white noise is added to the data before processing, to simulate noise generated by sensors.

This paper concerns the identification of nonlinear characteristics, and is based on the assumption that the underlying linear system is either known or can be found, for example using the methods proposed in [1]. Here, as the linear parameters of the system are known, see Table 1, this step is omitted.

Fig. 2 demonstrates the procedure that is used to find the backbone curves of system 1*NL*. The panels (a_1) and (a_2) show the experimental step of this procedure for the first and second backbone curves, labelled *S*1 and *S*2 respectively. Here, the system is forced at a constant amplitude and the forcing frequency, Ω_f, is varied such that the response may approach the backbone curves. As measurements of the forced responses are not required, the frequency, Ω_f, may be varied continuously in time. This results in lower experimental cost in comparison to techniques that require the system to reach steady-state between discrete frequency steps. Further details of how this may be achieved can be found in [24]. Once the response of the system is close to a backbone curve, the forcing is *released*, i.e. the forcing amplitude is set to zero, such that the transient response of the system then decays along, or close to, the backbone curve – see [24] for further details.

In panels (a_1) and (a_2), a thin-black line and dotted-green line show the forced response branches and backbone curves respectively. The paths taken along the forced response branches to approach the backbone curves are shown by a thick-black line and the points of release are represented by blue crosses. The points on the backbone curve along which the system response then decays are shown by large green dots (although here these points are illustrative and would not be realised in the frequency–amplitude projection until after the data-processing step).

The next step involves transforming the time-domain data describing the displacements of the physical coordinates, $\mathbf{x}$, into the displacements of the linear modal coordinates, $\mathbf{q}$. This step is necessary as the second-order normal form technique, used to generate an analytical model of the system, uses a linear modal transform to decouple the linear terms in the equation of motion, see Section 3 for further details. The linear modal displacements are found using the inverse linear modal transform, written as $\mathbf{q} = \mathbf{\Phi}^{-1}\mathbf{x}$ where $\mathbf{\Phi}$ is a modeshape matrix whose nth column describes the modeshape of the nth linear mode. Due to the symmetry of the underlying linear structure of the systems considered here, the modeshape matrix may be written as

$$\mathbf{\Phi} = \begin{bmatrix} 1 & 1 \\ 1 & -1 \end{bmatrix} \quad \text{such that } \mathbf{q} = \begin{pmatrix} q_1 \\ q_2 \end{pmatrix} = \frac{1}{2}\begin{pmatrix} x_1 + x_2 \\ x_1 - x_2 \end{pmatrix}. \tag{3}$$

Panels (b_1) and (b_2) in Fig. 2 show the transformed time-domain decay data for the backbone curves *S*1 and *S*2 respectively. Both panels are in the projection of time, t, against the modal displacements q_1 and q_2, where $q_1(t)$ and $q_2(t)$ are represented by solid-blue and dotted-red lines respectively. Embedded plots in these panels show a portion of the decay data in detail, and illustrate that for the decays along both backbone curves, the linear modes respond at the same frequency. Furthermore it can be seen in panel (b_1), showing *S*1, that linear modal coordinates are in anti-phase, and panel (b_2) shows that q_1 and q_2 are in-phase along *S*2.[1] This frequency and phase information is used later for the application of the second-order normal form technique.

The final step in the experimental acquisition of backbone curve involves the conversion of the time–displacement data into the frequency–amplitude domain. This is achieved using a moving-window discrete Fourier transform, with a window size of 5 periods, [25]. For the approach taken here the harmonic responses of this system are neglected and only the

[1] Note that q_1 and q_2 are linear modal coordinates. Panels (b_1) and (b_2) show how these modes contribute to the responses of the backbone curves *S*1 and *S*2 respectively.

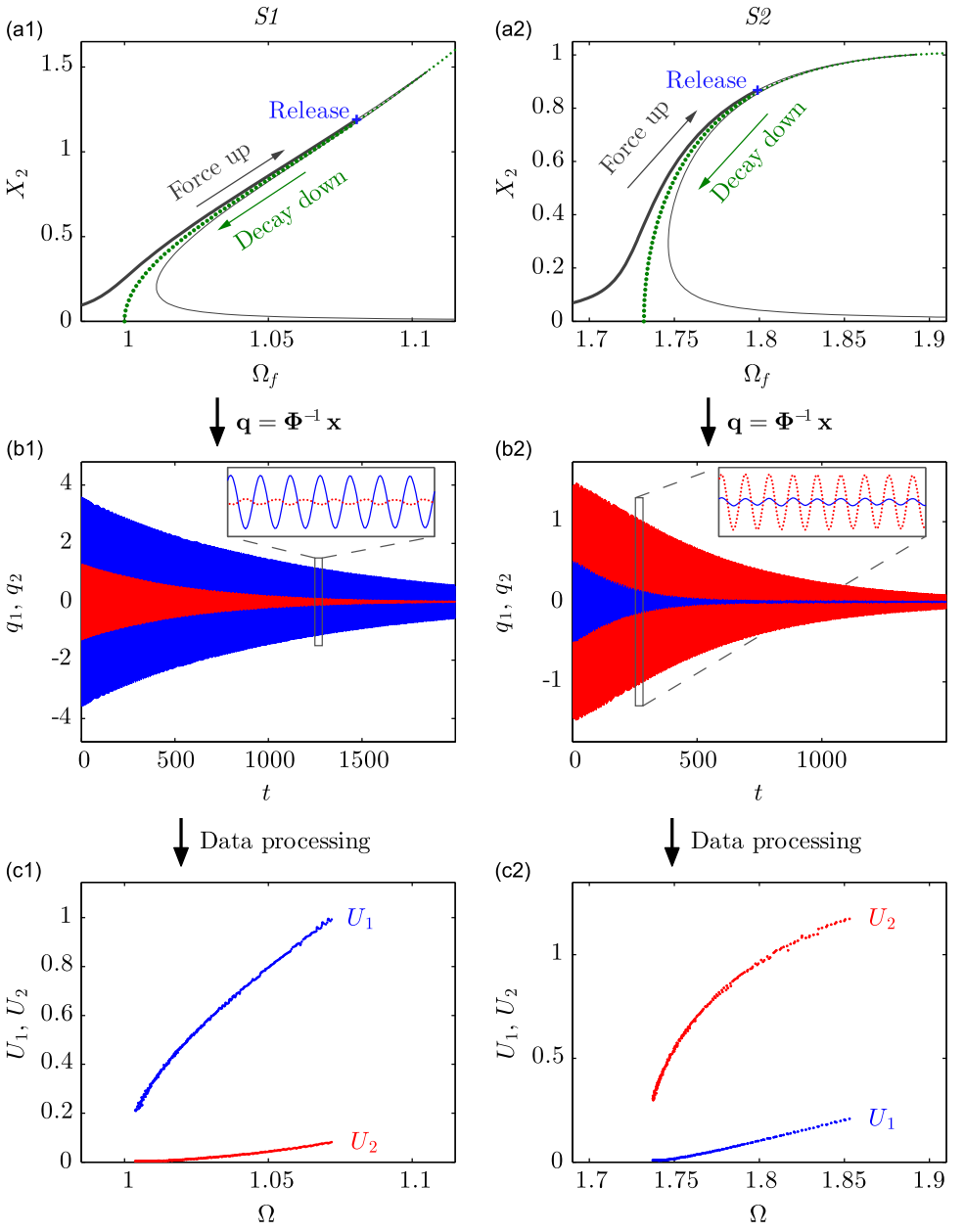

Fig. 2. A diagram of the procedure used to find the backbone curves of system 1*NL* through simulated experiment. The left-hand panels – labelled (a_1), (b_1) and (c_1) – and right-hand panels – labelled (a_2), (b_2) and (c_2) – depict the process of data acquisition for backbone curves *S*1 and *S*2 respectively.

fundamental responses are considered. The fundamental responses of q_1 and q_2 are denoted u_1 and u_2 respectively, and are assumed to be sinusoidal with frequency Ω and amplitudes U_1 and U_2 respectively – where Ω, the response frequency, is distinct from Ω_f, the forcing frequency. As the estimated frequency is likely to be more accurate for a signal of larger amplitude, and as it is known that both linear modes share response frequencies, the dominant mode is used to obtain the response frequency for both modes. It can be seen from panels (b_1) and (b_2) in Fig. 2 that $q_1 > q_2$ on *S*1 and $q_2 > q_1$ on *S*2.

Panels (c_1) and (c_2) in Fig. 2 show the frequency–amplitude data for backbone curves *S*1 and *S*2 respectively, and represent the data used for the identification of the nonlinear parameters in system 1*NL*. These are both shown in the projection of the common response frequency, Ω, against the fundamental response amplitudes, U_1 and U_2. Due to the noise applied to the time-domain signal, the translation into the frequency domain is inaccurate for low-amplitude signals. Therefore, the decay data along each of these backbone curves have been truncated as the low-amplitude mode approaches zero. As can be seen in panels (c_1) and (c_2), this results in the truncation of the dominant modes at relatively high amplitudes. The data are also truncated at the start of the decay in order to remove the transient effects as the response

converges towards the backbone curves. This transient behaviour is reduced if the system is released close to the backbone curve, allowing more high-amplitude data to be used for identification.

The systems considered here are discrete, however the same technique may be applied to continuous systems, provided that the linear modal displacements may be estimated. Additionally, as the technique presented here is concerned with identifying nonlinear parameters, only backbone curves that exhibit nonlinear behaviour, and their constituent linear modes, require experimental measurement [26]. This approach may be used to reduce the experimental and computational costs.

3. Calculating the backbone curves

To find the backbone curves of the system described by Eq. (1) the associated unforced, undamped dynamics are considered, which may be written as

$$\mathbf{M}\ddot{\mathbf{x}}+\mathbf{K}\mathbf{x}+\mathbf{\Gamma}_x(\mathbf{x})=0. \tag{4}$$

The second-order normal form technique is now used to transform the equation of motion, Eq. (4), into a set of time-invariant equations describing the backbone curves. An outline of the approach is given here, and a more detailed description is given in Appendix A. This approach is similar to that used in [20,21], and for a complete description of the second-order normal form technique, see [19]. This technique is limited to weakly nonlinear systems, i.e. the nonlinear terms are small relative to the linear terms. The error resulting from this assumption may be reduced by computing the technique to a higher order of accuracy [27].

As described in Section 2.2, the first step in the second-order normal form technique is the linear modal transform $\mathbf{x}=\mathbf{\Phi}\mathbf{q}$ where $\mathbf{\Phi}$ is a modeshape matrix which, for the systems considered here, is given in Eq. (3). Applying this transform to Eq. (4) allows us to write

$$\ddot{\mathbf{q}}+\mathbf{\Lambda}\mathbf{q}+\mathbf{N}_q(\mathbf{q})=0, \tag{5}$$

where $\mathbf{N}_q$ is a vector of nonlinear terms and $\mathbf{\Lambda}$ is a diagonal matrix whose nth diagonal term is the square of the nth linear natural frequency, ω_{nn}^2. For the systems considered here, one may write

$$\mathbf{\Lambda}=\begin{bmatrix}\omega_{n1}^2 & 0\\ 0 & \omega_{n2}^2\end{bmatrix}=\frac{1}{m}\begin{bmatrix}k_1 & 0\\ 0 & k_1+2k_2\end{bmatrix}, \tag{6}$$

and for both systems one may write

$$\mathbf{N}_q(\mathbf{q})=\frac{1}{2m}\begin{pmatrix}\alpha_1(q_1+q_2)^3+\alpha_3(q_1-q_2)^3\\ \alpha_1(q_1+q_2)^3+\alpha_3(q_2-q_1)^3+16\alpha_2q_2^3\end{pmatrix}. \tag{7}$$

The next step is to apply the nonlinear near-identity transform $\mathbf{q}=\mathbf{u}+\mathbf{h}$ where $\mathbf{u}$ and $\mathbf{h}$ describe the fundamental and harmonic contents of $\mathbf{q}$ respectively. Here, the harmonics are neglected as only the fundamental responses of the decay along the backbone curve are measured. However in Appendix A the harmonics are retained at this stage.

By removing the harmonics, one may write $\mathbf{q}=\mathbf{u}$, which may be substituted into Eq. (7), giving $\mathbf{N}_q(\mathbf{q})=\mathbf{N}_q(\mathbf{u})$. As it is assumed that the fundamental response of the nth linear mode, u_n, is sinusoidal, one may write

$$u_n=u_{np}+u_{nm}=\frac{U_n}{2}e^{+j(\Omega t-\phi_n)}+\frac{U_n}{2}e^{-j(\Omega t-\phi_n)}, \tag{8}$$

where U_n and ϕ_n are the amplitude and phase of u_n respectively. As, in the cases considered here, the linear modes respond at the same frequency (as shown in Fig. 2), both modes share the fundamental response frequency Ω. Note that the subscripts p and m correspond to the positive and negative (plus and minus) signs of the complex exponents respectively.

The nonlinear near-identity transform results in the resonant equation of motion, written as

$$\ddot{\mathbf{u}}+\mathbf{\Lambda}\mathbf{u}+\mathbf{N}_u(\mathbf{u})=0, \tag{9}$$

where $\mathbf{N}_u$ is a vector of resonant nonlinear terms – populated with the resonant terms from $\mathbf{N}_q(\mathbf{u})$. The process used to determine which terms in $\mathbf{N}_q(\mathbf{u})$ are resonant is detailed in Appendix A, where it is found that $\mathbf{N}_u(\mathbf{u})$ may be written as

$$\mathbf{N}_u=3\begin{pmatrix}\alpha_p\left[(u_{1p}u_{1m}+2u_{2p}u_{2m})u_1+u_{1p}u_{2m}^2+u_{1m}u_{2p}^2\right]+\alpha_m\left[(2u_{1p}u_{1m}+u_{2p}u_{2m})u_2+u_{1p}^2u_{2m}+u_{1m}^2u_{2p}\right]\\ \alpha_m\left[(u_{1p}u_{1m}+2u_{2p}u_{2m})u_1+u_{1p}u_{2m}^2+u_{1m}u_{2p}^2\right]+\alpha_p\left[(2u_{1p}u_{1m}+u_{2p}u_{2m})u_2+u_{1p}^2u_{2m}+u_{1m}^2u_{2p}\right]+8\frac{\alpha_2}{m}u_{2p}u_{2m}u_2\end{pmatrix}. \tag{10}$$

where $\alpha_p=(\alpha_1+\alpha_3)/2m$ and $\alpha_m=(\alpha_1-\alpha_3)/2m$. Substituting Eq. (10) into Eq. (9) forms the resonant equation of motion, in which all terms resonate at frequency Ω. As detailed in Appendix A, this can then be used to find the set of time-invariant equations describing the backbone curves which, for these systems, are given by

$$\left(\omega_{n1}^2-\Omega^2\right)U_1+\frac{3}{8m}\left[\alpha_1\left(U_1+pU_2\right)^3+\alpha_3\left(U_1-pU_2\right)^3\right]=0, \tag{11a}$$

$$\left(\omega_{n2}^2-\Omega^2\right)pU_2+\frac{3}{8m}\left[\alpha_1\left(U_1+pU_2\right)^3-\alpha_3\left(U_1-pU_2\right)^3+p16\alpha_2U_2^3\right]=0, \tag{11b}$$

where

$$p=\begin{cases}+1 & \text{when } \phi_1-\phi_2=0\\ -1 & \text{when } \phi_1-\phi_2=\pi\end{cases}, \tag{12}$$

i.e. $p=+1$ for backbone curves where the modes are in-phase, and $p=-1$ for backbone curves where the modes are in anti-phase.

Eqs. (11) and (12) are used in conjunction with the resonant decay data to identify the nonlinear parameters. The approach used for this has a Bayesian framework, as discussed in the following section.

Here, we find the parameters describing the equation of motion in the physical coordinates, Eq. (4); however, if one requires a modal model then the parameters describing the modal equation of motion, Eq. (5), may be identified.

4. Bayesian system identification

This section provides a brief overview of the Bayesian approach employed here, which uses the analytical expressions describing the backbone curves, Eq. (11), to form a physical-law based model $\mathcal{M}$. The model contains a vector of parameters $\boldsymbol{\theta}\in\boldsymbol{\Theta}\subset\mathbb{R}^{N_\theta}$ which require estimation (such that, in this case, $\boldsymbol{\theta}=\{\alpha_1,\alpha_2,\alpha_3\}$). These estimates are probabilistic such that future predictions made using $\mathcal{M}$ are robust against parameter uncertainties. Using the experimental data set, $\mathcal{D}$, consisting of the backbone curve data, the parameters, $\boldsymbol{\theta}$, are inferred. The probability of the parameters, $\boldsymbol{\theta}$, conditional on the model, $\mathcal{M}$, and the experimental data set, $\mathcal{D}$, can be obtained using Bayes' theorem:

$$P(\boldsymbol{\theta}|\mathcal{D},\mathcal{M})=\frac{P(\mathcal{D}|\boldsymbol{\theta},\mathcal{M})P(\boldsymbol{\theta}|\mathcal{M})}{P(\mathcal{D}|\mathcal{M})}, \tag{13}$$

where $P(\boldsymbol{\theta}|\mathcal{D},\mathcal{M})$ is the posterior distribution and $P(\boldsymbol{\theta}|\mathcal{M})$ – the prior – is a probability distribution describing one's knowledge of $\boldsymbol{\theta}$ before the data were known. The denominator of Eq. (13) can be interpreted as a normalising constant which ensures that the posterior integrates to unity, and is therefore defined as

$$P(\mathcal{D}|\mathcal{M})=\int_{\boldsymbol{\Theta}}P(\mathcal{D}|\boldsymbol{\theta},\mathcal{M})P(\boldsymbol{\theta}|\mathcal{M})\,\mathrm{d}\boldsymbol{\theta}. \tag{14}$$

The term $P(\mathcal{D}|\boldsymbol{\theta},\mathcal{M})$ is referred to as the likelihood and describes the probability of witnessing the data set $\mathcal{D}$ given that one *believes* that the behaviour of the real system can be replicated using model $\mathcal{M}$ with parameters $\boldsymbol{\theta}$. Evaluating Eq. (13) therefore requires the definition of a *prediction-error model* whose parameters can be included in $\boldsymbol{\theta}$.

In this case, the data set consists of K measurements of both U_1 and U_2, such that $\mathcal{D}=\{U_1^{(1)},\ldots,U_1^{(K)},U_2^{(1)},\ldots,U_2^{(K)}\}$. Assuming that the probabilities of witnessing separate data are always mutually independent and employing a Gaussian prediction-error model, the likelihood is

$$P(\mathcal{D}|\boldsymbol{\theta},\mathcal{M})\propto\prod_{i=1}^{K}\left\{\exp\left[-\frac{1}{2\sigma_1^2}\left(U_1^{(i)}-\hat{U}_1^{(i)}(\boldsymbol{\theta})\right)^2\right]\exp\left[-\frac{1}{2\sigma_2^2}\left(U_2^{(i)}-\hat{U}_2^{(i)}(\boldsymbol{\theta})\right)^2\right]\right\}, \tag{15}$$

where $\hat{U}_1$ and $\hat{U}_2$ represent predictions made by the model and σ_1 and σ_2 are parameters describing the standard deviations of the likelihood; which, in this case, are also included in $\boldsymbol{\theta}$. In its current form, evaluation of the likelihood requires one to assemble an explicit solution for $\hat{U}_1$ and $\hat{U}_2$ in terms of $\boldsymbol{\theta}$ – this can be algebraically demanding and may prevent the method proposed here from being applied to more complex systems. As an alternative, one can use the residuals of Eqs. (11), written as ϵ_1 and ϵ_2 and defined as

$$\left[\omega_{n1}^2-\left(\Omega^{(i)}\right)^2\right]U_1^{(i)}+\frac{3}{8m}\left[\alpha_1\left(U_1^{(i)}+pU_2^{(i)}\right)^3+\alpha_3\left(U_1^{(i)}-pU_2^{(i)}\right)^3\right]=\epsilon_1^{(i)}, \tag{16a}$$

$$\left[\omega_{n2}^2-\left(\Omega^{(i)}\right)^2\right]pU_2^{(i)}+\frac{3}{8m}\left[\alpha_1\left(U_1^{(i)}+pU_2^{(i)}\right)^3-\alpha_3\left(U_1^{(i)}-pU_2^{(i)}\right)^3+p16\alpha_2\left(U_2^{(i)}\right)^3\right]=\epsilon_2^{(i)}, \tag{16b}$$

where α_1, α_2 and α_3 are taken from elements of $\boldsymbol{\theta}$, and the data set is now defined as $\mathcal{D}=\{U_1^{(1)},\ldots,U_1^{(K)},U_2^{(1)},\ldots,U_2^{(K)},\boldsymbol{\Omega}^{(1)},\ldots,\boldsymbol{\Omega}^{(K)}\}$.

Deriving the probability of witnessing the residuals, given $\boldsymbol{\theta}$, is a complex problem. In this case the authors have chosen to use the *Principle of Maximum Entropy* [28] which states that, having defined its first two moments, choosing a likelihood of the form

$$P(\mathcal{D}|\boldsymbol{\theta},\mathcal{M})\propto\prod_{i=1}^{K}\left\{\exp\left[-\frac{1}{2\sigma_1^2}\left(\epsilon_1^{(i)}\right)^2\right]\exp\left[-\frac{1}{2\sigma_2^2}\left(\epsilon_2^{(i)}\right)^2\right]\right\}, \tag{17}$$

Table 2
The parameters limits used for the identification of systems 1*NL* and 3*NL*.

Parameter	Lower limit	Upper limit
α_1	0	3
α_2	0	3
α_3	0	3
σ_1	0	0.5
σ_2	0	0.5

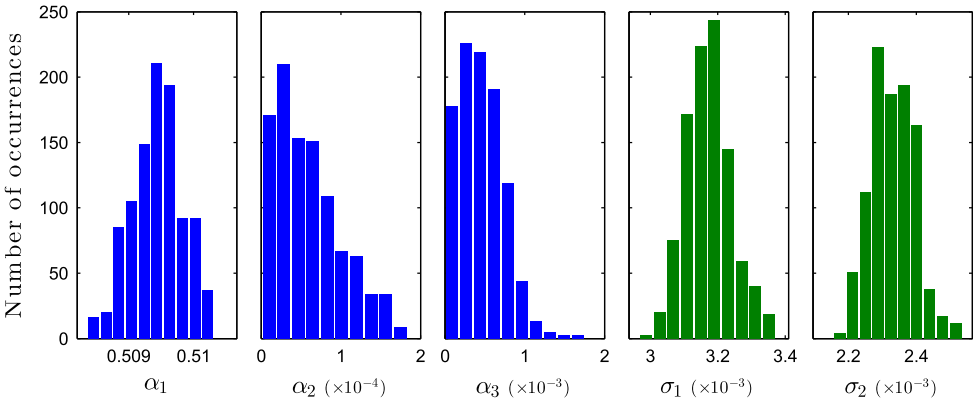

Fig. 3. Histograms, for system 1*NL*, showing the estimated values of the nonlinear parameters and the standard deviations of the residuals of the expressions describing the backbone curves. The nonlinear parameters, α_1, α_2 and α_3, are shown in blue and the standard deviations, σ_1 and σ_2, are shown in green. (For interpretation of the references to colour in this figure caption, the reader is referred to the web version of this paper.)

assumes the least amount of additional information. The consequences of selecting such a prediction-error model are discussed further in Section 5.2.

This reduces the complexity of the problem, as the residual terms, ϵ_1 and ϵ_2, can be found directly from the substitution of the data and parameters into Eqs. (16), without the need for algebraic manipulation. It is this approach that is adopted here, i.e. Eq. (17) is used to evaluate the likelihood. Furthermore we define the prior as having a uniform distribution.

With the likelihood and prior defined, the next task is to generate samples from the posterior distribution. In the current paper this is achieved through the use of Markov chain Monte Carlo (MCMC) methods[2] – algorithms which involve the evolution of an ergodic Markov chain whose stationary distribution is proportional to the posterior distribution (this is a particularly useful feature as it allows one to generate samples from $P(\boldsymbol{\theta}|\mathcal{D},\mathcal{M})$ whilst circumventing the need to evaluate the N_θ dimensional integral given by Eq. (14)). In this case, the authors employed a variant of the well-known Metropolis algorithm [29] detailed in [30].

It is important to note that, as each sample generated using MCMC requires a model run, the method proposed here is very computationally efficient, as each model run simply requires the evaluation of Eqs. (11). However, if one were attempting to infer parameter estimates using time history data, for example, each model run would require the numerical time-domain integration of the equations of motion of the system. The speed of the method proposed here is such that all of the MCMC simulations shown subsequently were conducted in a matter of seconds – this is without any parallel processing or the use of model emulators.

5. Parameter identification for the example systems

Here, a uniform prior distribution is utilised. Table 2 shows that the prior limits have been set such that the nonlinear parameters are positive, as the backbone curves depicted by the experimental data show a hardening nonlinear behaviour in both systems.

[2] Here, as Eqs. (16) are linear functions of the parameters, a suitable choice of prior would allow for closed-form expressions for the posterior. The authors have chosen to use MCMC as it demonstrates a method which can be applied in situations where such analytical treatment is not possible. It is expected that this will be the case when higher order approximations of the backbone curves are utilised [27] (a topic of future work).

5.1. Parameter identification for system 1NL

Fig. 3 shows histograms of the results of the identification procedure for system 1*NL*. Additionally, Table 3 shows, for each of the parameters, the true and mean estimated values along with the relative error of the mean estimated values. It can be seen from Fig. 3 that the variances of the estimated values of the nonlinear parameters are low. This indicates that the effects of these parameters are well-represented by the backbone curve data, and hence there is little uncertainty regarding their value.

Fig. 3 shows that the true value of α_1 (which is 0.5) is outside of the limits of the estimated values, whereas one would expect the true value to lie within these limits. The reason for this is that the second-order normal form technique, used to describe the backbone curves, is an approximate method. Therefore, the parameter estimates describe an optimisation of the fit between the true system and the approximate model, leading to the discrepancy between the true and estimated values. The relative error of α_1 is low, at less than 2 percent, suggesting a successful identification procedure. Additionally, the estimated values of α_2 and α_3 are very low suggesting that their identification was also accurate. For cases where there is a greater discrepancy between the true and the approximate model, the second-order normal form technique may be computed to a higher order of accuracy [27].

In order to investigate the significance of the error in the estimation of the nonlinear parameters, the backbone curves were calculated for both the true and estimated parameters using the numerical continuation software AUTO-07p [31]. These are shown in Fig. 4, where solid-green and dashed-red lines represent the backbone curves described by the true and estimated parameters respectively. It can be seen that the two sets of backbone curves are very similar and, importantly, it can also be seen that they are close at amplitude and response frequencies well-beyond those described by the data, which are represented by blue dots.

5.2. Uncertainty propagation for system 1NL

An advantage of the Bayesian analysis adopted here is that, using the samples generated by MCMC, it is possible to propagate the uncertainties in one's parameter estimates into future predictions. This involves conducting a Monte Carlo simulation, where each model run uses parameters from the vector $\boldsymbol{\theta}$, which have been sampled from the posterior parameter distribution (using MCMC). Recalling that $\boldsymbol{\theta}$ also includes parameters which were used to define the likelihood (σ_1 and σ_2 in this case), each model run is also "corrupted" with noise generated according to the prediction-error model

Table 3
The true and mean estimated parameter values, along with the relative error of the estimated values, for system 1*NL*.

Parameter	True value	Mean estimated value	Relative error
α_1	0.5	0.5094	1.887%
α_2	0	5.971×10^{-5}	–
α_3	0	4.524×10^{-4}	–
σ_1	–	3.173×10^{-3}	–
σ_2	–	2.330×10^{-3}	–

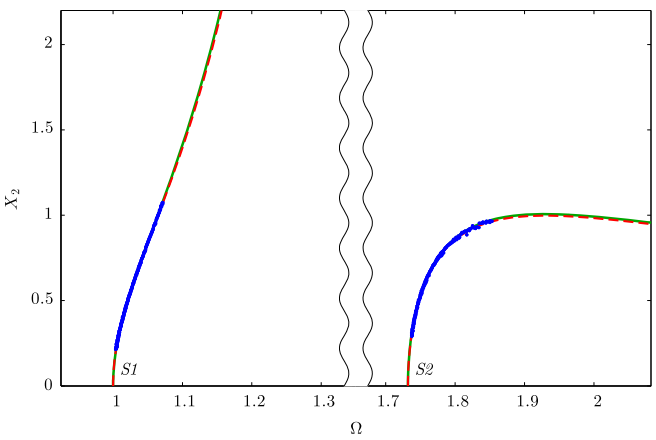

Fig. 4. The backbone curves *S*1 and *S*2 for system 1*NL*. These have been calculated using AUTO-07p (a numerical continuation package) for both the true and estimated parameters, represented by solid-green and dashed-red lines respectively. Blue dots show the data used for the identification of these parameters. These results are shown in the projection of the common response frequency, Ω, against the amplitude of displacement of the second mass, X_2. (For interpretation of the references to colour in this figure caption, the reader is referred to the web version of this paper.)

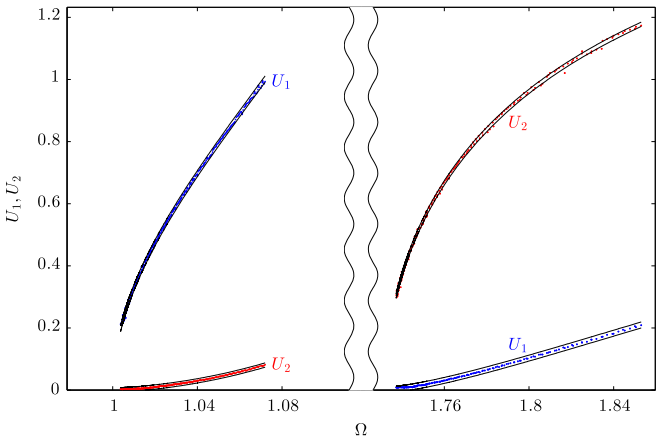

Fig. 5. Uncertainty propagation for the backbone curve decay data for system 1*NL*. This shows the backbone curve decay data in the projection of the fundamental response frequency, Ω, against the fundamental response amplitudes of the linear modal coordinates, U_1 and U_2. These are represented by blue and red dots respectively. The black lines show the confidence bounds at $\pm 3\sigma$. (For interpretation of the references to colour in this figure caption, the reader is referred to the web version of this paper.)

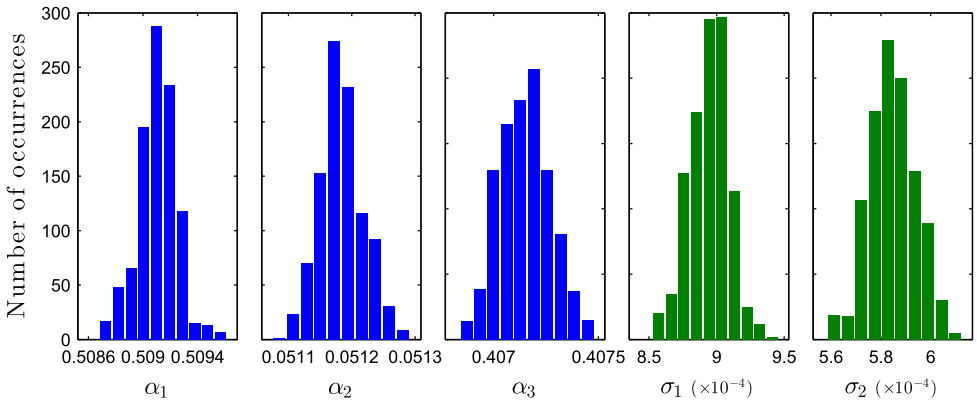

Fig. 6. Histograms, for system 3*NL*, showing the estimated values of the nonlinear parameters and the standard deviations of the residuals of the expressions describing the backbone curves. The nonlinear parameters, α_1, α_2 and α_3, are shown in blue and the standard deviations, σ_1 and σ_2, are shown in green. (For interpretation of the references to colour in this figure caption, the reader is referred to the web version of this paper.)

with parameters σ_1 and σ_2. Analysing the statistics of this ensemble of model predictions, Fig. 5 shows the $\pm 3\sigma$ confidence bounds that arose when predicting the backbone curves of system 1*NL*. It can be seen that, for the most part, the data are within the confidence bounds.

Any discrepancies (where data are outside the confidence bounds) may be due to erroneous assumptions about the prediction-error model. Specifically, for future work, the authors aim to investigate the assumption that the standard deviations of the prediction-error model are independent of the amplitude response of the system. This could involve analysing a set of different prediction-error models, thus allowing the probability of these competing models to assessed (also using a Bayesian framework) [32].

5.3. Parameter identification for system 3NL

The data used for the identification of system 3*NL* were also found through simulated experiment, in a similar procedure to that applied to system 1*NL*, as described in Section 2. The results of this are shown in Fig. 6, where the blue and green histograms show the identified values for the nonlinear parameters and standard deviations of the likelihood respectively. Table 4 also gives the true, mean estimated, and relative error for each of the parameters for system 3*NL*. As with system 1*NL*, the mean estimated values are very close to the true values and the low variance suggests a high confidence (i.e. the effects of the parameters are well-represented by the data). Also, the approximate nature of the model again results in true parameter values that lie outside of the limits of the estimated values.

Table 4 shows that the maximum relative error in the estimation of the nonlinear parameters is less than 2.5 percent. To test the influence of these errors, Fig. 7 shows the backbone curves for system 3*NL*, calculated using the numerical continuation software AUTO-07p, for both the true and estimated parameters. These are represented by solid-green and

Table 4
The true and mean estimated parameter values, along with the relative error of the estimated values, for system 3*NL*.

Parameter	True value	Mean estimated value	Relative error
α_1	0.5	0.5091	1.821%
α_2	0.05	0.05118	2.367%
α_3	0.4	0.4071	1.788%
σ_1	–	8.943×10^{-4}	–
σ_2	–	5.848×10^{-4}	–

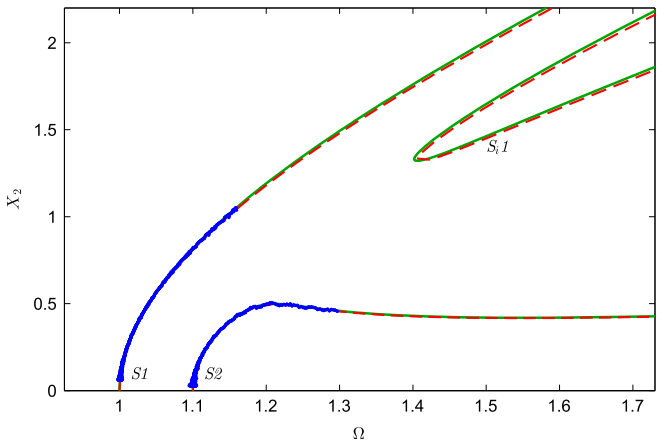

Fig. 7. The backbone curves *S*1 and *S*2, along with the isolated backbone curve S_i1, for system 3*NL*. These have been calculated using AUTO-07p (a numerical continuation package) for both the true and estimated parameters, represented by solid-green and dashed-red lines respectively. Blue dots show the data used for the identification of these parameters. These results are shown in the projection of the common response frequency, Ω, against the amplitude of displacement of the second mass, X_2. (For interpretation of the references to colour in this figure caption, the reader is referred to the web version of this paper.)

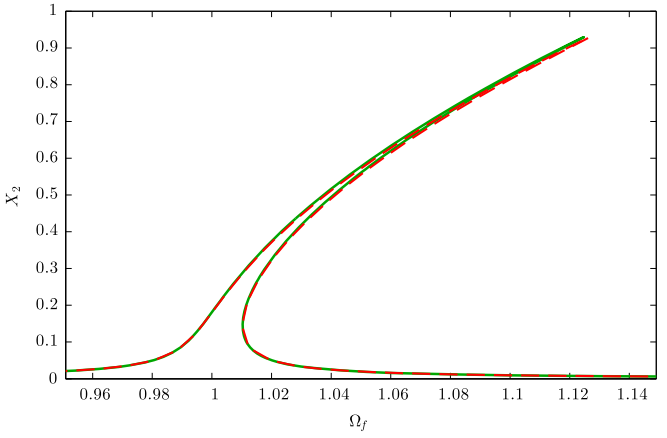

Fig. 8. The response of system 3*NL* when subjected to forcing at amplitude $\mathbf{P}_x^T = [0.002,\ 0.002]$. The solid-green line shows the response branch when the true nonlinear parameters are used, and the dashed-red line shows the response branch when the mean estimated parameters are used. These results are shown in the projection of forcing frequency, Ω_f, against the amplitude of displacement of the second mass, X_2. (For interpretation of the references to colour in this figure caption, the reader is referred to the web version of this paper.)

dashed-red lines respectively and blue dots show the data used for the identification of the parameters. One significant feature of these results is the detached backbone curve, denoted S_i1. This is referred to as an *isolated backbone curve*, and it can be viewed as an imperfect bifurcation of *S*2, caused by the asymmetry of this system. For further discussion of bifurcations in backbone curves see [20], and for discussion of isolated backbone curves see [33]. It can be seen that the system identification procedure used no data describing the backbone curve S_i1; despite this, Fig. 7 shows that S_i1 using the real and estimated parameters are close. This demonstrates that the estimated parameters lead to accurate predictions of the backbone curves, even for responses that are very distinct from those represented by the data.

5.4. Forced responses for system 3NL

Although backbone curves are of great value for understanding the fundamental properties of a nonlinear system, the forced responses are generally of greatest importance in engineering. Therefore, to further test the significance of the errors of the estimated parameters, the responses of the system when subjected to forcing are considered. Fig. 8 shows the response of system 3*NL* when subjected to forcing at amplitude $\mathbf{P}_x^T = [0.002, 0.002]$, such that forcing is applied directly to the first linear mode. Responses using both the true and mean estimated parameters are represented by a solid-green and a dashed-red line respectively. These results have been calculated using AUTO-07p [31]. As the forcing is only in the first linear mode, the response envelops the backbone curve $S1$ (in which the first mode is dominant) leading to a Duffing-like forced response when viewed in this projection. It can be seen in Fig. 8 that the forced response curve for the estimated parameters is very close to that which uses the true parameters, suggesting that the errors have little influence for the forcing considered here.

One significant property of an isolated backbone curve, such as S_i1 in Fig. 7, is that it may correspond to isolated forced solutions, or *isola*. These can be difficult to detect through experiment, or through modelling techniques that rely on continuation without prior knowledge of their existence, and hence isolas present significant challenges and potential risks in engineering [33,34]. Fig. 9 shows the forced responses of system 3*NL* using the estimated and true nonlinear parameters, represented by dashed-red and solid-green lines respectively. These are subjected to forcing at amplitude $\mathbf{P}_x^T = [0.01, -0.01]$, such that the forcing is applied directly to the second linear mode, and it can be seen that an isola exists, as indicated by the existence of S_i1. Fig. 9 also shows that the forced response branches are predicted accurately by the estimated parameters, even for those describing the isola, which exists well-away from the data used for estimation.

As, in this projection, the isola describes a high-amplitude response, predicting that its existence is important. Furthermore, reaching the isola experimentally would prove challenging, and hence, even if its existence is known, experimental data describing an isola are often not available for identification. Therefore, it is an important feature of identification methods to predict parameters with sufficient accuracy that they may, in turn, be used to predict the existence of such features, well-away from the available data.

6. Conclusions and future work

In this work, an approach for the Bayesian identification of the nonlinear parameters of dynamic structures has been introduced. This approach utilises the *backbone curves* of a system, which may be obtained experimentally, and modelled using analytical expressions derived using the second-order normal form technique. These analytical expressions are computationally efficient to evaluate, hence the identification procedure is carried out extremely rapidly. As such, the probabilistic estimation of the nonlinear parameters of two example cases demonstrated here – where each system has three unknown nonlinear parameters – is completed in a matter of seconds.

As discussed, one disadvantage of this approach is that the analytical expressions provide an *approximate* description of the backbone curves, thus introducing error into the model of the system. This is demonstrated in the results presented here, as the true values of the parameters lie outside of the range of estimated parameters. It is also demonstrated, however, that the resulting errors are small and their influence on the dynamic responses are negligible. This is shown through a comparison of the backbone curves of the systems using both the true and estimated parameter values, and shows a strong

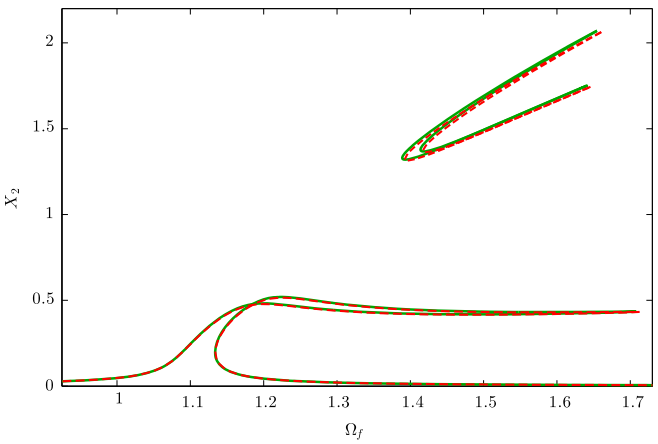

Fig. 9. The response of system 3*NL* when subjected to forcing at amplitude $\mathbf{P}_x^T = [0.01, -0.01]$. The solid-green line shows the response branches when the true nonlinear parameters are used, and the dashed-red line shows the response branches when the mean estimated parameters are used. These results are shown in the projection of forcing frequency, Ω_f, against the amplitude of displacement of the second mass, X_2. (For interpretation of the references to colour in this figure caption, the reader is referred to the web version of this paper.)

agreement at responses well-beyond those represented by the experimental data. Specifically, an *isolated backbone curve* is predicted for one case, and it is shown that this corresponds to an isola in the forced response of the system.

Not only has it been shown that this approach is extremely fast and accurate, it also lends itself to application to much larger systems. This is due to its use of analytical models, which remove the need for expensive numerical solving routines, and the use of the residuals of the expressions, which overcome the need to find explicit solutions. Additionally, the second-order normal form technique, used to find the analytical expressions for the backbone curves, has a matrix-based formulation that is well-suited to computer automation, hence allowing this approach to be extended to larger, more complex systems.

Acknowledgements

The authors would like to acknowledge the support of the EPSRC. T.L.H. is supported by an EPSRC DTA studentship. P.L.G. is supported by EPSRC Grant EP/K003836/1, A.C. is supported by EPSRC Grant EP/K003836/2 and S.A.N. is supported by EPSRC fellowship EP/K005375/1.

Appendix A. The method of second-order normal forms

The following description covers the steps of the second-order normal form technique that are necessary for the procedure followed in this paper. It is used to transform the unforced, undamped equations of motion, given by Eq. (4), into a set of time-invariant equations describing the backbone curves.

In Section 3 it is shown how the first step of the technique, the linear modal transform is applied to Eq. (4). This transforms the equations of motion from the physical coordinates, $\mathbf{x}$, into modal coordinates, $\mathbf{q}$, leading to the modal equation of motion, Eq. (5), in which the linear terms are decoupled. The next step of the second-order normal form technique, for unforced systems, is the nonlinear near-identity transform. This transform takes the form $\mathbf{q}=\mathbf{u}+\varepsilon\mathbf{h}$ where $\mathbf{u}$ and $\mathbf{h}$ describe the fundamental and harmonic contents of $\mathbf{q}$ respectively, and ε is used to denote *smallness*. In this case ε is used to indicate that the harmonics are small, relative to the fundamental responses. As it is also assumed that the nonlinear terms are small, one may write $\mathbf{N}_q(\mathbf{q})=\varepsilon\mathbf{N}_q(\mathbf{q})$. Therefore, applying the transform $\mathbf{q}=\mathbf{u}+\varepsilon\mathbf{h}$ to $\mathbf{N}_q(\mathbf{q})$ allows us to make the order ε^1 approximation $\varepsilon\mathbf{N}_q(\mathbf{u}+\varepsilon\mathbf{h})\approx\varepsilon\mathbf{N}_q(\mathbf{u})$.

As described in Section 3, the nth fundamental response is written as

$$u_n=u_{np}+u_{nm}=\frac{U_n}{2}\mathrm{e}^{+\mathrm{j}(\Omega t-\phi_n)}+\frac{U_n}{2}\mathrm{e}^{-\mathrm{j}(\Omega t-\phi_n)}, \tag{A.1}$$

where U_n and ϕ_n are the amplitude and phase of u_n respectively, and Ω is the fundamental response frequency, common to both linear modes. The substitution of $q_n=u_n=u_{np}+u_{nm}$ into $\mathbf{N}_q(\mathbf{q})$ is now made, using Eq. (A.1) and the description of $\mathbf{N}_q(\mathbf{q})$ given in Eq. (7). This substitution leads to

$$\mathbf{N}_q(\mathbf{u})=\frac{1}{2m}\begin{pmatrix}\alpha_1(u_{1p}+u_{1m}+u_{2p}+u_{2m})^3+\alpha_3(u_{1p}+u_{1m}-u_{2p}-u_{2m})^3\\ \alpha_1(u_{1p}+u_{1m}+u_{2p}+u_{2m})^3+\alpha_3(u_{2p}+u_{2m}-u_{1p}-u_{1m})^3+16\alpha_2(u_{2p}+u_{2m})^3\end{pmatrix}. \tag{A.2}$$

The purpose of the nonlinear near-identity transform is to find the resonant equation of motion, written as

$$\ddot{\mathbf{u}}+\mathbf{\Lambda}\mathbf{u}+\mathbf{N}_u(\mathbf{u})=0, \tag{A.3}$$

where $\mathbf{N}_u(\mathbf{u})$ is a vector populated with the resonant terms from $\mathbf{N}_q(\mathbf{u})$. In order to determine which terms in $\mathbf{N}_q(\mathbf{u})$ are resonant, $\mathbf{N}_q(\mathbf{u})=[n_q]\mathbf{u}^*$ is found, where $\mathbf{u}^*$ is a vector of all unique combinations of u_{np} and u_{nm}, and $[n_q]$ is a matrix containing all coefficients of the corresponding terms. In the case considered here, there are 20 unique terms in $\mathbf{N}_q(\mathbf{u})$. Using this, the ℓ th element of $\mathbf{u}^*$ is written as

$$u^*_\ell=\prod_{k=1}^{2}\left\{u_{kp}^{s_{k\ell p}}u_{km}^{s_{k\ell m}}\right\}, \tag{A.4}$$

where $s_{k\ell p}$ and $s_{k\ell m}$ are the exponents of u_{kp} and u_{km} respectively. Substituting Eq. (A.1) into Eq. (A.4), u^*_ℓ may be written as

$$u^*_\ell=\left[\prod_{k=1}^{2}\left(\frac{U_k}{2}\right)^{(s_{k\ell p}+s_{k\ell m})}\right]\mathrm{e}^{\mathrm{j}\left(\overline{\omega}_\ell t-\overline{\phi}_\ell\right)}, \tag{A.5}$$

where $\overline{\phi}_\ell$ and $\overline{\omega}_\ell$ are the phase and response frequency of u^*_ℓ respectively, and are found using

$$\overline{\phi}_\ell=\sum_{k=1}^{2}(s_{k\ell p}-s_{k\ell m})\phi_k,\quad \overline{\omega}_\ell=\left[\sum_{k=1}^{2}(s_{k\ell p}-s_{k\ell m})\right]\Omega. \tag{A.6}$$

The matrix $\boldsymbol{\beta}$ is now introduced in order to determine which of these terms are resonant (i.e. $|\overline{\omega}_\ell| = \Omega$). The $\{n, \ell\}$ th element of $\boldsymbol{\beta}$ is written as

$$\beta_{n,\ell} = \overline{\omega}_\ell^2 - \Omega^2 = \left\{ \left[\sum_{k=1}^{2} \left(s_{k\ell p} - s_{k\ell m} \right) \right]^2 - 1 \right\} \Omega^2. \tag{A.7}$$

It can be seen that any element in $\boldsymbol{\beta}$ with a value of zero must correspond to an element in $[n_q]$ that describes the coefficient of a resonant term. Hence, one may define the matrix $[n_u]$ which is equal in size to $[n_q]$ and whose elements are populated by the coefficients of the resonant terms, such that

$$[n_u]_{n\ell} = \begin{cases} [n_q]_{n\ell} & \text{if } \beta_{n\ell} = 0, \\ 0 & \text{if } \beta_{n\ell} \neq 0. \end{cases} \tag{A.8}$$

From this, the vector of nonlinear terms – see Eq. (A.3) – is defined using $\mathbf{N}_u = [n_u]\mathbf{u}^*$, where all terms in $\mathbf{N}_u$ resonate at frequency Ω.

From Eqs. (A.2), (A.4) and (A.7), $[n_q]$, $\mathbf{u}^*$ and $\boldsymbol{\beta}$ are calculated as

$$[n_q]^T = \begin{bmatrix} \alpha_p & \alpha_m \\ 3\alpha_p & 3\alpha_m \\ 3\alpha_p & 3\alpha_m \\ \alpha_p & \alpha_m \\ 3\alpha_p & 3\alpha_m \\ 3\alpha_p & 3\alpha_m \\ 6\alpha_p & 6\alpha_m \\ 6\alpha_p & 6\alpha_m \\ 3\alpha_p & 3\alpha_m \\ 3\alpha_p & 3\alpha_m \\ 3\alpha_m & 3\alpha_p \\ 3\alpha_m & 3\alpha_p \\ 6\alpha_m & 6\alpha_p \\ 6\alpha_m & 6\alpha_p \\ 3\alpha_m & 3\alpha_p \\ 3\alpha_m & 3\alpha_p \\ \alpha_m & \tilde{\alpha} \\ 3\alpha_m & 3\tilde{\alpha} \\ 3\alpha_m & 3\tilde{\alpha} \\ \alpha_m & \tilde{\alpha} \end{bmatrix}, \quad \mathbf{u}^* = \begin{bmatrix} u_{1p}^3 \\ u_{1p}^2 u_{1m} \\ u_{1p} u_{1m}^2 \\ u_{1m}^3 \\ u_{1p} u_{2p}^2 \\ u_{1m} u_{2p}^2 \\ u_{1p} u_{2p} u_{2m} \\ u_{1m} u_{2p} u_{2m} \\ u_{1p} u_{2m}^2 \\ u_{1m} u_{2m}^2 \\ u_{1p}^2 u_{2p} \\ u_{1p}^2 u_{2m} \\ u_{1p} u_{1m} u_{2p} \\ u_{1p} u_{1m} u_{2m} \\ u_{1m}^2 u_{2p} \\ u_{1m}^2 u_{2m} \\ u_{2p}^3 \\ u_{2p}^2 u_{2m} \\ u_{2p} u_{2m}^2 \\ u_{2m}^3 \end{bmatrix}, \quad \boldsymbol{\beta}^T = \Omega^2 \begin{bmatrix} 8 & 8 \\ 0 & 0 \\ 0 & 0 \\ 8 & 8 \\ 8 & 8 \\ 0 & 0 \\ 0 & 0 \\ 0 & 0 \\ 0 & 0 \\ 8 & 8 \\ 8 & 8 \\ 0 & 0 \\ 0 & 0 \\ 0 & 0 \\ 0 & 0 \\ 8 & 8 \\ 8 & 8 \\ 0 & 0 \\ 0 & 0 \\ 8 & 8 \end{bmatrix}, \tag{A.9}$$

where $\alpha_p = (\alpha_1 + \alpha_3)/2m$, $\alpha_m = (\alpha_1 - \alpha_3)/2m$ and $\tilde{\alpha} = \alpha_p + 8\alpha_2/m$. Now, from Eqs. (A.8) and (A.9), and using $\mathbf{N}_u = [n_u]\mathbf{u}^*$, $\mathbf{N}_u$ may be written as

$$\mathbf{N}_u = 3 \begin{pmatrix} \alpha_p \left[(u_{1p}u_{1m} + 2u_{2p}u_{2m})u_1 + u_{1p}u_{2m}^2 + u_{1m}u_{2p}^2 \right] + \alpha_p \alpha_m \left[(2u_{1p}u_{1m} + u_{2p}u_{2m})u_2 + u_{1p}^2 u_{2m} + u_{1m}^2 u_{2p} \right] \\ \alpha_m \left[(u_{1p}u_{1m} + 2u_{2p}u_{2m})u_1 + u_{1p}u_{2m}^2 + u_{1m}u_{2p}^2 \right] + \alpha_p \left[(2u_{1p}u_{1m} + u_{2p}u_{2m})u_2 + u_{1p}^2 u_{2m} + u_{1m}^2 u_{2p} \right] + 8\frac{\alpha_2}{m} u_{2p}u_{2m}u_2 \end{pmatrix}. \tag{A.10}$$

Substituting Eq. (A.10) into the resonant equation of motion, Eq. (A.3), it can be seen that all terms are sinusoidal and resonating at frequency Ω. Therefore it follows that

$$\left[\left(\boldsymbol{\Lambda} - \Omega^2 \mathbf{I} \right) \mathbf{u}_p + \mathbf{N}_u^+ \right] e^{+j\Omega t} + \left[\left(\boldsymbol{\Lambda} - \Omega^2 \mathbf{I} \right) \mathbf{u}_m + \mathbf{N}_u^- \right] e^{-j\Omega t} = 0, \tag{A.11}$$

where $\mathbf{I}$ is the identity matrix, and $\mathbf{u}_p$, $\mathbf{u}_m$, $\mathbf{N}_u^+$ and $\mathbf{N}_u^-$ form two sets of complex conjugate vector pairs, given by

$$\mathbf{u}_p = \frac{1}{2} \begin{pmatrix} U_1 e^{-j\phi_1} \\ U_2 e^{-j\phi_2} \end{pmatrix}, \quad \mathbf{u}_m = \frac{1}{2} \begin{pmatrix} U_1 e^{+j\phi_1} \\ U_2 e^{+j\phi_2} \end{pmatrix},$$
$$\text{and} \quad \mathbf{N}_u = \mathbf{N}_u^+ e^{+j\Omega t} + \mathbf{N}_u^- e^{-j\Omega t}. \tag{A.12}$$

From Eq. (A.11), it can be seen that

$$\left(\boldsymbol{\Lambda} - \Omega^2 \mathbf{I} \right) \mathbf{u}_p + \mathbf{N}_u^+ = 0, \tag{A.13}$$

where from Eq. (A.10)

$$\mathbf{N}_u^+ = \begin{pmatrix} \frac{3}{8}\left\{\alpha_p\left[U_1^3+U_1U_2^2\left(2+e^{+j2\phi_d}\right)\right]+\alpha_m\left[U_2^3+U_1^2U_2\left(2+e^{-j2\phi_d}\right)\right]e^{+j\phi_d}\right\}e^{-j\phi_1} \\ \frac{3}{8}\left\{\alpha_p\left[U_2^3+U_1^2U_2\left(2+e^{-j2\phi_d}\right)\right]+\alpha_m\left[U_1^3+U_1U_2^2\left(2+e^{+j2\phi_d}\right)\right]e^{-j\phi_d}+8\frac{\alpha_2}{m}U_2^3\right\}e^{-j\phi_2} \end{pmatrix}, \tag{A.14}$$

where $\phi_d = \phi_1 - \phi_2$. Substituting Eqs. (A.12) and (A.14) into Eq. (A.13) gives

$$\left(\omega_{n1}^2-\Omega^2\right)U_1+\frac{3}{4}\left\{\alpha_p\left[U_1^3+U_1U_2^2\left(2+e^{+j2\phi_d}\right)\right]+\alpha_m\left[U_2^3+U_1^2U_2\left(2+e^{-j2\phi_d}\right)\right]e^{+j\phi_d}\right\}=0, \tag{A.15a}$$

$$\left(\omega_{n2}^2-\Omega^2\right)U_2+\frac{3}{4}\left\{\alpha_p\left[U_2^3+U_1^2U_2\left(2+e^{-j2\phi_d}\right)\right]+\alpha_m\left[U_1^3+U_1U_2^2\left(2+e^{+j2\phi_d}\right)\right]e^{-j\phi_d}+8\frac{\alpha_2}{m}U_2^3\right\}=0. \tag{A.15b}$$

Taking the imaginary parts of Eqs. (A.15) shows that $\sin(\phi_d)=0$. Therefore $e^{\pm j2\phi_d}=1$ and $e^{\pm j\phi_d}=\pm 1=p$, such that when $p=+1$ the two modes are in-phase, and when $p=-1$ the two modes are in anti-phase, as seen in Section 2.2. This allows Eqs. (A.15) to be written as

$$\left(\omega_{n1}^2-\Omega^2\right)U_1+\frac{3}{8m}\left[\alpha_1\left(U_1+pU_2\right)^3+\alpha_3\left(U_1-pU_2\right)^3\right]=0, \tag{A.16a}$$

$$\left(\omega_{n2}^2-\Omega^2\right)pU_2+\frac{3}{8m}\left[\alpha_1\left(U_1+pU_2\right)^3-\alpha_3\left(U_1-pU_2\right)^3+p16\alpha_2U_2^3\right]=0, \tag{A.16b}$$

where $\alpha_p=(\alpha_1+\alpha_3)/2m$ and $\alpha_m=(\alpha_1-\alpha_3)/2m$ have been used.

References

[1] J.R. Write, J.E. Cooper, M.J. Desforges, Normal-mode force appropriation—theory and application, *Mechanical Systems and Signal Processing* 13 (2) (1999) 217–240.

[2] D.J. Ewins, *Modal Testing: Theory, Practice, and Application, Mechanical Engineering Research Studies: Engineering Dynamics Series*, Research Studies Press, 2000.

[3] G. Kerschen, J.-C. Golinval, K. Worden, Theoretical and experimental identification of a non-linear beam, *Journal of Sound and Vibration* 244 (4) (2001) 597–613, http://dx.doi.org/10.1006/jsvi.2000.3490.

[4] S.A. Billings, *Nonlinear System Identification: NARMAX Methods in the Time, Frequency, and Spatio-Temporal Domains*, Wiley, Chichester, UK, 2013.

[5] G. Kerschen, J.-C. Golinval, Generation of accurate finite element models of nonlinear systems – application to an aeroplane-like structure, *Nonlinear Dynamics* 39 (1–2) (2005) 129–142, http://dx.doi.org/10.1007/s11071-005-1919-8.

[6] G. Kerschen, K. Worden, A.F. Vakakis, J.-C. Golinval, Past, present and future of nonlinear system identification in structural dynamics, *Mechanical Systems and Signal Processing* 20 (3) (2006) 505–592, http://dx.doi.org/10.1016/j.ymssp.2005.04.008.

[7] M. Feldman, Identification of weakly nonlinearities in multiple coupled oscillators, *Journal of Sound and Vibration* 303 (12) (2007) 357–370, http://dx.doi.org/10.1016/j.jsv.2007.01.028.

[8] M.F. Platten, J.R. Wright, J.E. Cooper, G. Dimitriadis, Identification of a nonlinear wing structure using an extended modal model, *Journal of Aircraft* 46 (5) (2009) 1614–1626, http://dx.doi.org/10.2514/1.42024.

[9] K.-V. Yuen, J.L. Beck, Updating properties of nonlinear dynamical systems with uncertain input, *Journal of Engineering Mechanics* 129 (1) (2003) 9–20.

[10] M. Muto, J.L. Beck, Bayesian updating and model class selection for hysteretic structural models using stochastic simulation, *Journal of Vibration and Control* 14 (1–2) (2008) 7–34.

[11] K. Worden, J.J. Hensman, Parameter estimation and model selection for a class of hysteretic systems using Bayesian inference, *Mechanical Systems and Signal Processing* 32 (2012) 153–169, http://dx.doi.org/10.1016/j.ymssp.2012.03.019. Special Issue: Uncertainties in Structural Dynamics.

[12] P.L. Green, Bayesian system identification of a nonlinear dynamical system using a novel variant of simulated annealing, *Mechanical Systems and Signal Processing* 52-53 (2015) 133–146, http://dx.doi.org/10.1016/j.ymssp.2014.07.010.

[13] J. Ching, Y. Chen, Transitional Markov chain Monte Carlo method for Bayesian model updating, model class selection, and model averaging, *Journal of Engineering Mechanics* 133 (7) (2007) 816–832, http://dx.doi.org/10.1061/(ASCE)0733-9399(2007)133:7(816).

[14] P. Angelikopoulos, C. Papadimitriou, P. Koumoutsakos, Bayesian uncertainty quantification and propagation in molecular dynamics simulations: a high performance computing framework, *The Journal of Chemical Physics* 137 (14). http://dx.doi.org/10.1063/1.4757266.

[15] P.L. Green, E.J. Cross, K. Worden, Bayesian system identification of dynamical systems using highly informative training data, Mechanical Systems and Signal Processing 56-57, 2015, 109-122, 10.1016/j.ymssp.2014.10.003.

[16] A. Tondl, T. Ruijgrok, F. Verhulst, R. Nabergoj, *Autoparametric Resonance in Mechanical Systems*, Cambridge University Press, 2000.

[17] P. Glendinning, *Stability, Instability and Chaos: An Introduction to the Theory of Nonlinear Differential Equations, Cambridge Texts in Applied Mathematics*, Cambridge University Press, 1994.

[18] L. Jezequel, C.H. Lamarque, Analysis of non-linear dynamical systems by the normal form theory, *Journal of Sound and Vibration* 149 (3) (1991) 429–459 , http://dx.doi.org/10.1016/0022-460X(91)90446-Q.

[19] S.A. Neild, D.J. Wagg, Applying the method of normal forms to second-order nonlinear vibration problems, *Proceedings of the Royal Society A: Mathematical, Physical and Engineering Science* 467 (2011) 1141–1163, http://dx.doi.org/10.1098/rspa.2010.0270.

[20] A. Cammarano, T.L. Hill, S.A. Neild, D.J. Wagg, Bifurcations of backbone curves for systems of coupled nonlinear two mass oscillator, *Nonlinear Dynamics* 77 (1–2) (2014) 311–320, http://dx.doi.org/10.1007/s11071-014-1295-3.

[21] T.L. Hill, A. Cammarano, S.A. Neild, D.J. Wagg, Out-of-unison resonance in weakly nonlinear coupled oscillators, *Proceedings of the Royal Society of London A: Mathematical, Physical and Engineering Sciences* 471 (2173) (2014). http://dx.doi.org/10.1098/rspa.2014.0659.

[22] G. Kerschen, M. Peeters, J.C. Golinval, A.F. Vakakis, Nonlinear normal modes, Part I: *a useful framework for the structural dynamicist*, *Mechanical Systems and Signal Processing* 23 (1) (2009) 170–194. Special Issue: Non-linear Structural Dynamics. http://dx.doi.org/10.1016/j.ymssp.2008.04.002.

[23] MATLAB, version 8.1.0 (R2013a), The MathWorks Inc., Natick, Massachusetts, 2013.

[24] J.M. Londoño, S.A. Neild, J.E. Cooper, Identification of backbone curves of nonlinear systems from resonance decay responses, Journal of Sound and Vibration 348, 2015, 224-238, 10.1016/j.jsv.2015.03.015.

[25] S.A. Neild, P.D. McFadden, M.S. Williams, A review of time-frequency methods for structural vibration analysis, *Engineering Structures* 25 (6) (2003) 713–728, http://dx.doi.org/10.1016/S0141-0296(02)00194-3.
[26] M.F. Platten, J.R. Wright, G. Dimitriadis, J.E. Cooper, Identification of multi-degree of freedom non-linear systems using an extended modal space model, *Mechanical Systems and Signal Processing* 23 (1) (2009) 8–29.
[27] S. Neild, D. Wagg, A generalized frequency detuning method for multidegree-of-freedom oscillators with nonlinear stiffness, *Nonlinear Dynamics* 73 (1–2) (2013) 649–663, http://dx.doi.org/10.1007/s11071-013-0818-7.
[28] E.T. Jaynes, *Probability Theory: The Logic of Science*, Cambridge University Press, 2003.
[29] N. Metropolis, A.W. Rosenbluth, M.N. Rosenbluth, A.H. Teller, E. Teller, Equation of state calculations by fast computing machines, *The Journal of Chemical Physics* 21 (6) (1953) 1087–1092, http://dx.doi.org/10.1063/1.1699114.
[30] P.L. Green, Bayesian system identification of nonlinear dynamical systems using a fast MCMC algorithm, in: *Proceedings of ENOC 2014, European Nonlinear Dynamics Conference*, 2014.
[31] E.J. Doedel, with major contributions from A.R. Champneys, T.F. Fairgrieve, Yu.A. Kuznetsov, F. Dercole, B.E. Oldeman, R.C. Paffenroth, B. Sandstede, X.J. Wang, C. Zhang, AUTO-07P: Continuation and Bifurcation Software for Ordinary Differential Equations, Concordia University, Montreal, Canada, Available at: http://cmvl.cs.concordia.ca/, 2008.
[32] E. Simoen, C. Papadimitriou, G. Lombaert, On prediction error correlation in Bayesian model updating, *Journal of Sound and Vibration* 332 (18) (2013) 4136–4152.
[33] R. Kuether, L. Renson, T. Detroux, C. Grappasonni, G. Kerschen, M. Allen, Nonlinear normal modes modal interactions and isolated resonance curves, *Journal of Sound and Vibration* 351 (2015) 299–310, http://dx.doi.org/10.1016/j.jsv.2015.04.035.
[34] N.A. Alexander, F. Schilder, Exploring the performance of a nonlinear tuned mass damper, *Journal of Sound and Vibration* 319 (12) (2009) 445–462, http://dx.doi.org/10.1016/j.jsv.2008.05.018.